PHYSICAL REVIEW C **86**, 034613 (2012)

Decay of ^{241}Pu* formed in ^{9}Be + ^{232}Th around the Coulomb barrier using static and dynamic deformations

Gudveen Sawhney, Raj Kumar, and Manoj K. Sharma
School of Physics and Materials Science, Thapar University, Patiala 147004, India

(Received 26 May 2012; revised manuscript received 4 September 2012; published 25 September 2012)

The decay of the hot and rotating compound nucleus ^{241}Pu* formed in the reaction ^{9}Be + ^{232}Th around the Coulomb barrier (≈42.16 MeV), at energies ranging from 37 to 48 MeV, is studied using the dynamical cluster-decay model (DCM) with the effects of static and dynamic deformations included. With the inclusion of dynamical deformations both the preformation probability P_0 and the tunneling probability P, and hence the cross sections, change considerably. The only parameter of the model, namely, the neck-length parameter, varies smoothly with excitation energy or temperature of the system both at above- and below-barrier energies, whose value depends strongly on the limiting angular momentum, which in turn depends on the sticking and nonsticking moments of inertia. The relative effect of static and dynamic deformations on the neck-length parameter ΔR is also studied which indicates the reaction time scale for both static and dynamic choices of deformation. In addition, the exclusive role of angular momentum and "barrier modification" effects at sub-barrier energies are also addressed. Although calculated anisotropies are consistent with the results of Appannababu *et al.* [Phys. Rev. C **83**, 067601 (2011)], no significant contribution of a noncompound nucleus in the form of incomplete fusion is seen on the basis of DCM calculations.

DOI: 10.1103/PhysRevC.86.034613 PACS number(s): 25.70.Jj, 23.70.+j, 24.10.−i, 27.90.+b

I. INTRODUCTION

Fusion reactions induced by weakly bound projectiles have contributed immensely in the development and understanding of nuclear reaction dynamics in recent years. These reactions are sensitive not only to the entrance channel of interacting heavy ions forming the compound nucleus but also to the other aspects of the intermediate composite as it equilibrates in energy, mass, angular momentum, and orientation degrees of freedom. The entrance channel properties of the reacting systems such as target deformation, entrance channel Coulomb repulsion, and in particular mass-asymmetry play a major role in compound-nucleus-based nuclear reaction dynamics as well as for non-compound-nucleus processes such as quasifission (QF), incomplete fusion (ICF), deep inelastic collision (DIC), etc. It is well known that the entrance channel mass asymmetry η [$=(A_T - A_P)/(A_T + A_P)$, where A_T and A_P are the target and projectile mass, respectively] with respect to the Businaro-Gallone critical mass asymmetry α_{BG} plays an important role in the reaction dynamics [1,2]. Several measurements involving reactions with lighter projectiles such as ^{6,7}Li, ^{9}Be, ^{10,11}B, and ^{12}C on deformed actinide targets have shown that the anisotropies exceed the standard statistical saddle-point model (SSPM) predictions by large amounts, at sub-barrier energies. This anomalous behavior of the fragment anisotropies has been a subject of extensive investigations both experimentally and theoretically in the recent past. It was reported in Ref. [3] that anomalous fragment anisotropies in case of highly fissile target nuclei arise due to an admixture of compound-nucleus (CN) fission along with non-compound-nucleus (nCN) fission events in the form of QF, ICF, or DIC. Various models such as the pre-equilibrium fission model of Ramamurthy and Kapoor [3,4] and entrance-channel-dependent (ECD) K-state model by Vorkapic and Ivanisevic [5] were proposed to explain the anomalous fission fragment angular distribution for the systems having contribution from non-compound-nucleus fission. A systematic study [6] on the behavior of the stable weakly bound projectiles ^{6,7}Li and ^{9}Be on heavy targets such as ^{208}Pb and ^{209}Bi was made and it was observed that complete fusion (CF) is suppressed by around 30%. This fusion suppression was observed to be associated with the presence of ICF.

Recently, a ^{9}Be beam has been used and fission fragment anisotropies, together with fission excitation functions, have been measured for the compound nucleus ^{241}Pu* formed by the ^{9}Be + ^{232}Th reaction over a wide range of energies spread around the Coulomb barrier [7]. As expected, σ_{fiss} for the highly fissile ^{241}Pu* is the major contributor to the total decay cross sections and the contribution from the evaporation residue (ER) cross section σ_{ER} is not measured in [7]. Comparison of anisotropy data for the CN ^{241}Pu* is in good accord with the predictions of SSPM at above-barrier energies but show significant deviations for energies below the barrier. The higher anisotropy observed for the ^{9}Be + ^{232}Th reaction cannot be explained in terms of other reaction mechanisms such as quasifission since it takes place for more symmetric systems and usually for projectiles heavier than $A = 20$ [8]. Also for this system $\eta > \alpha_{BG}$, and therefore deviation of the fission fragment angular distribution from statistical theory is not expected on the basis of the pre-equilibrium fission model [3,4]. Thus, the noted deviation in the measured anisotropy data from SSPM predictions seems to be associated with the possible breakup of the loosely bound ^{9}Be projectile nucleus as suggested in Ref. [7].

In the present work we have applied the dynamical cluster-decay model (DCM) of Gupta and collaborators [9–22] to study the decay of the odd compound system ^{241}Pu* ($\alpha_{BG} = 0.882$) formed in the ^{9}Be + ^{232}Th ($\eta = 0.925$) reaction [7].

The projectile, the target, and the compound nucleus formed are all strongly deformed so the role of deformation and orientation effects is expected to be important in the context of the present study. The calculations are performed for deformed fragments using quadrupole (β_2) deformations having "optimum" orientations θ^{opt} taken from Table I of Ref. [23] and the higher multipole deformations (β_2-β_4) having "compact" orientations θ^c of hot configurations [24]. In addition, the possible fragmentation path in reference to temperature-dependent (dynamic) deformations [25,26] is also worked out in the framework of DCM to analyze the possible role of temperature-dependent deformations in the reaction under consideration. The dynamic deformations disappear exponentially as a function of temperature. This means that with the increase in temperature (T), the effect of dynamic deformations decreases and approaches zero at higher temperature. It is observed that with the inclusion of temperature-dependent (dynamic) deformations of the decaying fragments, the potential energy surface (PES) changes quite significantly and as a result the relative preformation probabilities P_0 for all fragments gets modified accordingly. Also the scattering potential (corresponding barrier position, height, and frequency) is modified with the inclusion of temperature-dependent deformations of outgoing fragments, thereby affecting the tunneling probability P through the barrier.

In this paper we use the data of Ref. [7] to fix the only parameter of DCM, the "neck-length parameter" ΔR. For deformations up to β_2 (quadrupole), the fission distribution remains asymmetric for both static and dynamic deformation cases, whereas a small contribution of symmetric fission is also observed when higher order static deformation effects up to β_4 (hexadecapole) are included. The calculated fission-fragment anisotropies are found to be consistent with the SSPM and pre-equilibrium fission (PEQ) model predictions at above-barrier energies, but calculations fail to reproduce the same at near- and below-barrier energies, in agreement with [7]. The main aim of this paper is (i) to study the role of static and dynamic deformations in the decay of $^{241}\text{Pu}^*$ using the DCM at both below- and above-barrier energies; (ii) to identify the time scale at which fission fragments are emitted for static and dynamic choice of deformations; (iii) to investigate the barrier modification effect, particularly in the below-barrier region, as such an effect is known to be important for resolving the issue of fusion hindrance in coupled channel calculations; (iv) to investigate fission anisotropies in the context of the $^9\text{Be} + {}^{232}\text{Th}$ reaction; and (v) to explore the possibility of an nCN competing channel, if any, on the basis of the DCM. This information is expected to impart important information for overall understanding of fusion-fission dynamics involved in weakly bound reactions.

The organization of the paper is as follows: A brief account of the DCM for a hot and rotating compound nucleus, with effects of deformations and orientations of the two nuclei or fragments included, is presented in Sec. II. The results of our calculations for both the fission excitation functions and the fission fragment anisotropies are discussed in Sec. III. Finally, the results are summarized in Sec. IV.

II. THE DYNAMICAL CLUSTER-DECAY MODEL

The DCM [9–22], an adaptation of the preformed-cluster model for ground-state decays [27–29], is based on dynamical (or quantum-mechanical) fragmentation theory. It is worked out in terms of the collective coordinates of mass and charge asymmetries

$$\eta = \frac{A_1 - A_2}{A_1 + A_2} \quad \text{and} \quad \eta_Z = \frac{Z_1 - Z_2}{Z_1 + Z_2},$$

the relative separation R, multipole deformations $\beta_{\lambda i}$ ($\lambda = 2, 3, 4, \ldots; i = 1, 2$), and orientations θ_i ($i = 1, 2$) of two nuclei or fragments. Here 1 and 2 stand, respectively, for heavy and light fragments. For the decay of a compound nucleus, the coordinates η and R refer, respectively, to nucleon division (or nucleon exchange) between the outgoing fragments and the transfer of kinetic energy of the incident channel ($E_{\text{c.m.}}$) to the internal excitation of the outgoing channel. By using these coordinates, in terms of the ℓ partial waves, the compound nucleus decay or the fragment formation cross section is given by

$$\sigma = \sum_{\ell=0}^{\ell_{\max}} \sigma_\ell = \frac{\pi}{k^2} \sum_{\ell=0}^{\ell_{\max}} (2\ell + 1) P_0 P, \quad k = \sqrt{\frac{2\mu E_{\text{c.m.}}}{\hbar^2}}, \tag{1}$$

where the preformation probability P_0 refers to η motion and the penetrability P to R motion. $\mu = [A_1 A_2/(A_1 + A_2)]m = \frac{1}{4} Am(1 - \eta^2)$ is the reduced mass with m as the nucleon mass. $\ell_{\max}$ is that value of angular momentum at which the preformation factor for light particles becomes negligibly small. Both P_0 and P depend on ℓ, T, $\beta_{\lambda i}$, and θ_i of the two nuclei.

The preformation probability $P_0(A_i) = \sqrt{B_{\eta\eta}} |\psi[\eta(A_i)]|^2 (2/A)$, $i = 1$ or 2, is the solution of the stationary Schrödinger equation in η, at fixed $R = R_a$, the first turning point of the penetration path shown in Fig. 1 of Ref. [13]. Thus P_0 contains the structure information of the compound nucleus that enters via the fragmentation potential

$$\begin{aligned} V_R(\eta, T) &= \sum_{i=1}^{2} [V_{\text{LDM}}(A_i, Z_i, T)] + \sum_{i=1}^{2} [\delta U_i] \exp\left(-T^2/T_0^2\right) \\ &\quad + V_C(R, Z_i, \beta_{\lambda i}, \theta_i, T) + V_P(R, A_i, \beta_{\lambda i}, \theta_i, T) \\ &\quad + V_\ell(R, A_i, \beta_{\lambda i}, \theta_i, T). \end{aligned} \tag{2}$$

Here V_P, V_C, and V_ℓ are the temperature-dependent nuclear proximity, Coulomb, and angular-momentum-dependent potentials, respectively, for deformed and oriented nuclei. V_{LDM} is the T-dependent liquid drop energy of Davidson *et al.* [30], with its constants at $T = 0$ refitted [31] to give recent experimental binding energies [32], and δU, the "empirical" shell corrections, from Myers and Swiatecki [33], approaches zero exponentially with T. $T_0 = 1.5$ MeV from the classical work of Jensen and Damgaard [34], which means that the shell correction term becomes nearly zero for $T > 4$ MeV. Note that the highest temperature is 1.27 MeV in reference to available data, and hence the shell correction effects seem important. It is to be noted that so far we have used static deformations $\beta_{\lambda i}$

($\lambda = 2, 3, 4$) taken from the theoretical estimates of Möller *et al.* [35] in the framework of the DCM. However, in general, static deformation of the nucleus has its origin in shell effects and at high excitation energies the shell effects vanish and thus static deformation should approach zero [25,26,34]. So in order to simulate this effect the deformation parameter β_i is taken to be temperature dependent in the DCM by using the relation [25,26]

$$\beta_{\lambda i}(T) = \exp(-T/T_0)\beta_{\lambda i}(0), \quad i = 1, 2, \tag{3}$$

where $\beta_{\lambda i}(0)$ is the static deformation and T_0 is the temperature of the nucleus at which shell effects start to vanish ($T_0 =$ 1.5 MeV) [25]. Thus the choice of temperature-dependent deformation parameter is consistent with static deformation when the temperature approaches zero, i.e., $T \to 0$. The mass parameters $B_{\eta\eta}(\eta)$ entering the P_0 calculation are taken as the smooth classical hydrodynamical masses [36], used for reasons of simplicity. The T-dependent nuclear proximity for deformed, oriented nuclei [37] is given by

$$V_p(s_0(T)) = 4\pi \bar{R}(T)\gamma b(T)\Phi(s_0(T)), \tag{4}$$

where $b(T) = 0.99(1 + 0.009T^2)$ is the nuclear surface thickness, $\gamma = 0.9517[1 - 1.7826(\frac{N-Z}{A})^2]$ MeV fm^{-2} is the surface energy constant, and $\overline{R}(T)$ is the mean curvature radius. Φ in Eq. (4) is a universal function; it is independent of the shapes of the nuclei or the geometry of the nuclear system, but it depends on the minimum separation distance $s_0(T)$ (for details see Ref. [37]).

The Coulomb potential for a multipole-multipole interaction between two separated nuclei is given by

$$\begin{aligned} V_C(R, A_i, \beta_{\lambda i}, \theta_i, T) &= Z_1 Z_2 e^2/R(T) + 3Z_1Z_2e^2 \\ &\quad \times \sum_{\lambda, i=1,2} \frac{R_i^{\lambda}(\alpha_i, T)}{(2\lambda+1)R(T)^{\lambda+1}} Y_{\lambda}^{(0)}(\theta_i) \\ &\quad \times \left\{\beta_{\lambda i} + \frac{4}{7}\left[\beta_{\lambda i}^2 Y_{\lambda}^{(0)}(\theta_i)\right]\right\}, \end{aligned} \tag{5}$$

and the centrifugal potential is

$$V_\ell(R, A_i, \beta_{\lambda i}, \theta_i, T) = \frac{\hbar^2 \ell(\ell+1)}{2I(T)}, \tag{6}$$

with $I = I_S = \mu R^2 + \frac{2}{5}A_1 m R_1^2(\alpha_1, T) + \frac{2}{5}A_2 m R_2^2(\alpha_2, T)$, the moment of inertia in the sticking limit, or, alternatively, the one calculated in the nonsticking limit $I = I_{NS} = \mu R^2$.

The penetrability P in Eq. (1) is the WKB integral

$$P = \exp\left(-\frac{2}{\hbar}\int_{R_a}^{R_b} \{2\mu[V(R) - Q_{\text{eff}}]\}^{1/2} dR\right), \tag{7}$$

with R_b as the second turning point satisfying $V(R_a, \ell) = V(R_b, \ell) = Q_{\text{eff}}(T, \ell) = TKE(T)$. The first turning point R_a, taken to be the same for all ℓ values, is defined as

$$\begin{aligned} R_a &= R_1(\alpha_1, T) + R_2(\alpha_2, T) + \Delta R(T) \\ &= R_t(\alpha, T) + \Delta R(T), \end{aligned} \tag{8}$$

with the radius vectors ($i = 1, 2$)

$$R_i(\alpha_i, T) = R_{0i}(T)\left[1 + \sum_{\lambda} \beta_{\lambda i} Y_{\lambda}^{(0)}(\alpha_i)\right], \tag{9}$$

where the temperature-dependent nuclear radii $R_{0i}(T)$ are taken from the work of [38] and are given by

$$R_{0i}(T) = \left[1.28A_i^{1/3} - 0.76 + 0.8A_i^{-1/3}\right](1 + 0.0007T^2). \tag{10}$$

T (in MeV) is calculated from $E_{\text{c.m.}}$ and the incoming Q value, since the CN excitation energy $E^* = E_{\text{c.m.}} + Q_{\text{in}} = (A_{CN}/a)T^2 - T$ with the level density parameter $a = 9$–11, depending on the mass A_{CN} of the compound nucleus. In the present calculations, we have taken $a = 9$.

$\Delta R(T)$ in Eq. (8) is the neck-length parameter that assimilates the neck formation effects between two nuclei and is similar to that used in both the scission-point [39] and saddle-point [40,41] statistical fission models. The choice of parameter R_a (equivalently, ΔR) for the best fit to the data corresponds to the effects of "barrier lowering" in it for each decay channel, defined for each ℓ as the difference between V_B^{ℓ} and $V^{\ell}(R_a)$, the barrier height and the actually used barrier, as

$$\Delta V_B^{\ell} = V^{\ell}(R_a) - V_B^{\ell}. \tag{11}$$

Finally, the dependence of anisotropy on different quantities can also be explored through the DCM within the SSPM approach [42],

$$A = 1 + \langle \ell^2 \rangle / 4K_0^2, \tag{12}$$

where K_0^2 is the variance of the K distribution and $\langle \ell^2 \rangle$ is the mean square angular momentum of the fissioning nucleus related to the total ℓ value (equivalently, ℓ_{max} of the compound nucleus). Here, K_0^2 is related to the effective moment of inertia of the compound nucleus, I_{eff}, and the saddle-point temperature T by

$$K_0^2 = T \times I_{\text{eff}}/\hbar^2.$$

I_{eff} is calculated by using the finite-range rotating liquid drop model [43] with T being the temperature of the fissioning nucleus. The value of ℓ_{max} depends on the use of I_S or I_{NS} in the centrifugal potential explained in Eq. (6).

The preference of I_S over I_{NS} in the calculations of fission cross section is discussed through the variation of the centrifugal potential in Fig. 1 calculated at a fixed ℓ value for the decay of ^{241}Pu$^{*} \to {}^{232}$Th + ^{9}Be using static deformations (β_{2i} alone) having the "optimum" hot orientations of Ref. [23]. It is observed that there is large difference in the magnitude of the centrifugal potential within the range of the reaction dynamics (i.e., ~8 to 14 fm). The I_{NS} approximation gives a large centrifugal potential as compared to I_S at the same R. Since we are using a proximity interaction in our model the use of I_S is justified as the structure effects due to proximity forces are more visible for the sticking moment of inertia. It may be noted that the use of I_{NS} in the centrifugal potential weakens the nuclear proximity interaction (attractive) and hence a $V_\ell(I_S)$ with a relatively lower magnitude is preferred. On the other hand, the fission anisotropies are calculated by using an I_{eff} based on the finite-range liquid drop model [43] and proximity forces are not involved in these calculations, so the use of the I_{NS} limit is more appropriate.

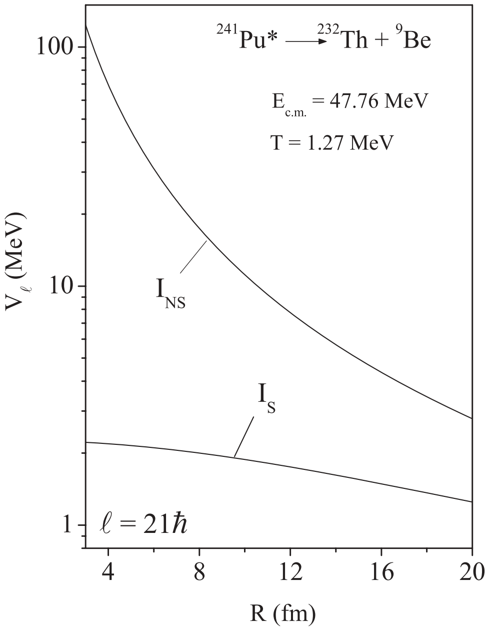

FIG. 1. The variation of centrifugal potential V_ℓ with two choices of sticking I_S and nonsticking I_{NS} limits of moment of inertia for the ^{241}Pu* → ^{232}Th + ^{9}Be reaction calculated at the highest $E_{\text{c.m.}} = 47.76$ MeV for $\ell = 21\hbar$.

III. CALCULATIONS AND DISCUSSION

In this section, we study the characteristics of decay barrier height, potential energy surfaces, preformation probability, penetrability, and barrier-lowering effect using the DCM, for both static and dynamic deformations in the decay of the compound nucleus ^{241}Pu* formed in the ^{9}Be + ^{232}Th reaction. The angular momentum dependence of the above-mentioned variables is studied to get fission excitation functions to be compared with experimental data [7]. These calculations are performed for the sticking moment of inertia I_S, which is found to be more appropriate for obtaining the fission cross sections which involve a comparatively larger limiting $\ell_{\max}$ value, whereas the nonsticking moment of inertia I_{NS} is found more appropriate for anisotropy calculations [14].

The scattering potentials in Fig. 2, at fixed $T = 1.27$ MeV (equivalently, $E_{\text{c.m.}} = 47.76$ MeV) for $\ell = 0$ and $\ell_{\max}$ cases, show that the barrier position as well as barrier height get modified with the inclusion of deformation and orientation degree of freedom, thereby affecting the tunneling probability. Solid lines are for spherical shapes, and dashed and dotted lines are with static and dynamic choices of quadrupole deformation parameter β_2 alone. Note that the calculated compound-nucleus-decay cross section in the DCM depends on penetrability P as given by Eq. (1), and hence on the deformations and orientations of nuclei. Similarly, the fact that the orientation degree of freedom θ modifies the barrier strongly is illustrated in Fig. 3 for the $\ell = 0$ case.

In order to see the relative effect of static and dynamic deformations, we have plotted the (decay) barrier height V_B as a function of light fragment mass A_2 for the decay of ^{241}Pu* formed in the ^{9}Be + ^{232}Th reaction at two different ℓ values in Fig. 4, with deformation effects included up to quadrupole deformation β_2 alone. It is clearly evident that the decay barrier height (V_B) increases as a function of fragment mass, independent of static and dynamic deformations. This behavior is similar to that observed for the static deformations in the decay of the heavy compound systems ^{215}Fr* and ^{204}Po* [14,19]. The

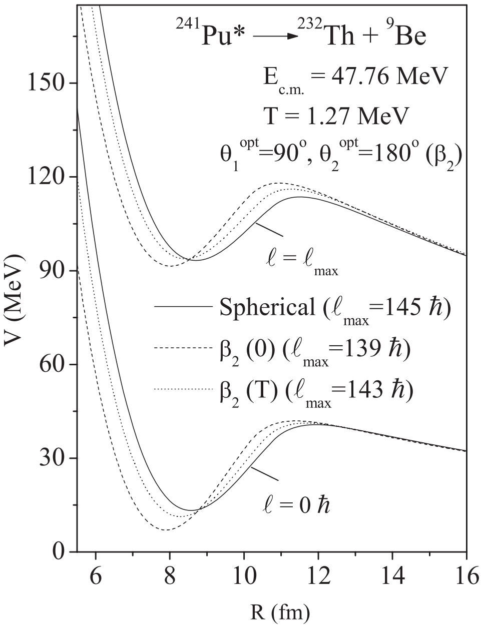

FIG. 2. The scattering potential $V(R)$ for the decay of ^{241}Pu* → ^{232}Th + ^{9}Be at $E_{\text{c.m.}} = 47.76$ MeV calculated at $\ell = 0$ and $\ell_{\max}$ with both fragments taken with static and dynamic considerations up to β_{2i} alone having the "optimum" hot orientations θ_i^{opt} of Table I in Ref. [23].

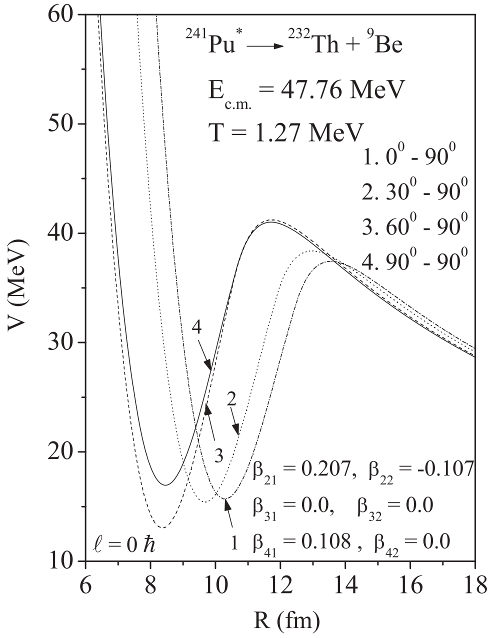

FIG. 3. Scattering potential $V(R)$ for the ^{241}Pu* → ^{232}Th + ^{9}Be reaction at various illustrative orientations for the case of static multipole deformations included up to hexadecapole at $\ell = 0$.

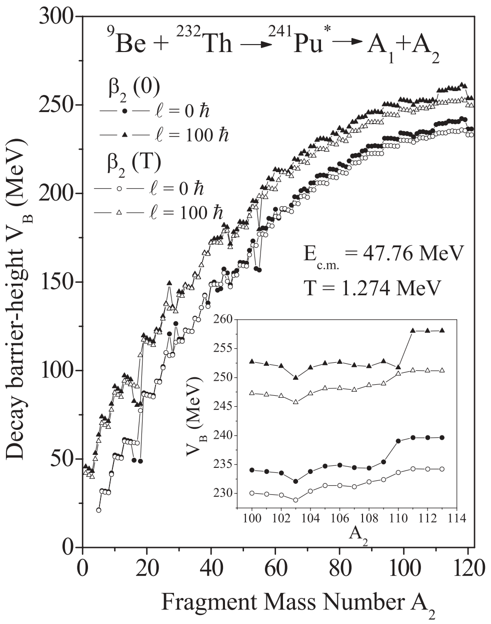

FIG. 4. The barrier height V_B as a function of light fragment mass (A_2), for the decay of ^{241}Pu* formed in the ^{9}Be + ^{232}Th reaction, calculated at two different ℓ values for both static and dynamic choices of deformation up to quadrupole (β_2) alone.

V_B distribution for the fission window with fragments $A_2 =$ 100–113, chosen to fit the respective experimental data [7], is more pronounced at both $\ell = 0$ and $\ell = 100\hbar$ values, as shown in the inset of Fig. 4. One can clearly see that V_B decreases, and hence the decay probability increases, with the inclusion of dynamical deformations in the decay of ^{241}Pu*. In other words, the decay barrier height is strongly influenced with the inclusion of static and dynamic deformations for a heavy nuclear system having fission as its prominent decay channel. Therefore a comprehensive study of static and dynamic deformations in the fragmentation process of a nuclear system may impart useful information in the context of nuclear reaction dynamics.

Figure 5 shows the fragmentation potential $V(A)$, minimized in mass coordinate η_A, at the two extreme ℓ values plotted on either side of the Coulomb barrier ($E_{\text{c.m.}} =$ 37.13 MeV and $E_{\text{c.m.}} = 47.76$ MeV), for the ^{9}Be + ^{232}Th reaction. Here we have plotted the cases of static and dynamic deformations up to quadrupole deformation β_2 alone [panels (a) and (b)], as well as for higher multipole deformations up to hexadecapole (β_2-β_4) [panels (c) and (d)]. These calculations are made for different neck-length parameters ΔR, chosen to fit the experimental data on fission cross sections.

We notice the following interesting results in Fig. 5:

(i) The fragmentation potentials are quite similar for both static and dynamic deformations up to β_2 alone, except for the fissioning region. Also some extra valleys at ^{17}B and ^{26}Mg fragments are observed for the case of $\beta_2(0)$ [Figs. 5(a) and 5(b)], but they get ruled out in calculations due to their negligible penetrability P values.

(ii) With the inclusion of temperature dependence in higher multipole deformations (β_2-β_4) of the decaying fragments, the PES changes significantly for $A_2 > 50$ and hence the relative preformation probability P_0 for all

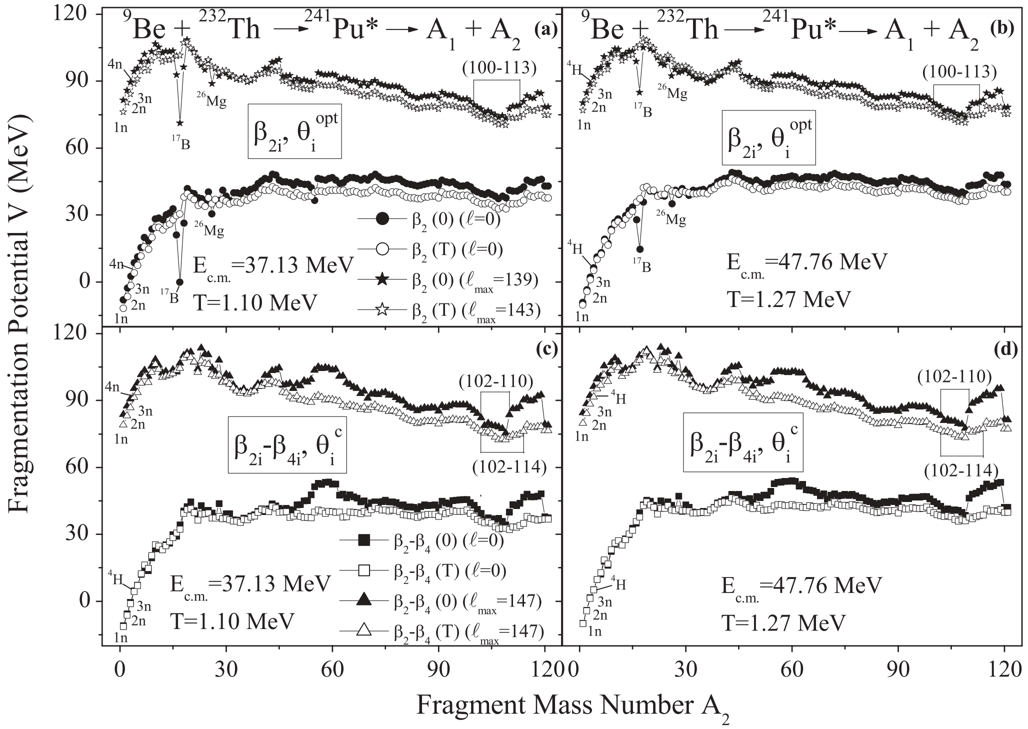

FIG. 5. Fragmentation potentials $V(A_2)$ as a function of fragment mass number A_2 for the decay of ^{241}Pu*, plotted at extreme $\ell(\hbar)$ values, for both static and dynamic choices of deformation up to quadrupole (β_2) alone and hexadecapole (β_2-β_4) deformed fragments.

fragments would change accordingly. However, there is no noticeable change in the structure of $V(A_2)$ up to $A_2 = 50$, except in the characteristics of emitted light particle (LPs).

(iii) The contributing LP(s) change in going from $\ell = 0$ to $\ell_{\max}$ with the inclusion of higher multipole deformations up to β_4 [Fig. 5(c)]. However, the result does not remain consistent with the increase in energy from below to above the barrier.

(iv) The ER contribution ($A_2 \leqslant 4$) is prominent (lower in energy) at $\ell = 0$ whereas at $\ell = \ell_{\max}$ the fission fragments start dominating in the decay process.

(v) The $\ell_{\max}$ value remains the same over a wide range of incident energies for both static and dynamic cases for the β_2 deformed case as well as for β_2-β_4 deformed fragments.

The above results are investigated further in terms of the preformation probability P_0 plotted as a function of fragment mass number ($A_i, i = 1, 2$) (see Fig. 6). We notice from Figs. 5(a) and 5(b) and 6(a) and 6(b) that for the β_2-deformed choice of nuclei, asymmetric fragmentation is preferred for both static and dynamic deformations, and the fragments in the mass range $A_2 = 100$–113 (plus complementary heavy fragments) contribute toward fission fragments. In other words, the fragmentation behavior remains asymmetric for both cases over the range of energy under consideration, although one may see some contribution of symmetric fission fragments as well but its magnitude is negligibly small. With the inclusion of higher multipole deformations (β_2-β_4) of the decaying fragments, the relative preformation probability P_0 shows some variation, as is evident from Figs. 6(c) and 6(d). The distribution yield is asymmetric for static as well as dynamic deformations just like that for the β_2-deformed case. Here again some symmetric fragments are prominent for the β_2-$\beta_4(0)$ case. In other words, some symmetric fragments are appearing particularly in the static deformed case, and their contribution seems more prominent for higher order deformations and at higher incident energies. The emergence of a symmetric mass distribution along with the observed asymmetric fragmentation indicates a possible fine structure in the fission of the ^{241}Pu* nucleus.

For a further analysis of different fission regions we have shown in Fig. 7 the symmetric fission (SF) peak to asymmetric fission (AF) peak ratio plotted as a function of $E_{\text{c.m.}}$ for the static higher multipole deformations (β_2-β_4) of the decaying fragments. Here the AF peak corresponds to fragment mass $A_2 = 102$–110 and the SF peak corresponds to $A_2 = 120$ at all measured energies. In order to predict the relative contribution of the SF to AF peak ratio at higher energies, the ΔR values are obtained by extrapolating the fitted ΔR values for the measured fission cross sections. It is clear from Fig. 7 that the symmetric fission region contributes a very small amount, though nonzero ($\sim$1.6%), to the FF (fusion fission) cross section at the highest extrapolated center-of-mass energy in comparison to $\sim$0.63% at the highest available $E_{\text{c.m.}}$ (=47.76 MeV), which signifies the asymmetric fragmentation path in the decay of the ^{241}Pu* nuclear system. These differences in the fission valley structure of fragmentation potentials or, equivalently, in preformation yields due

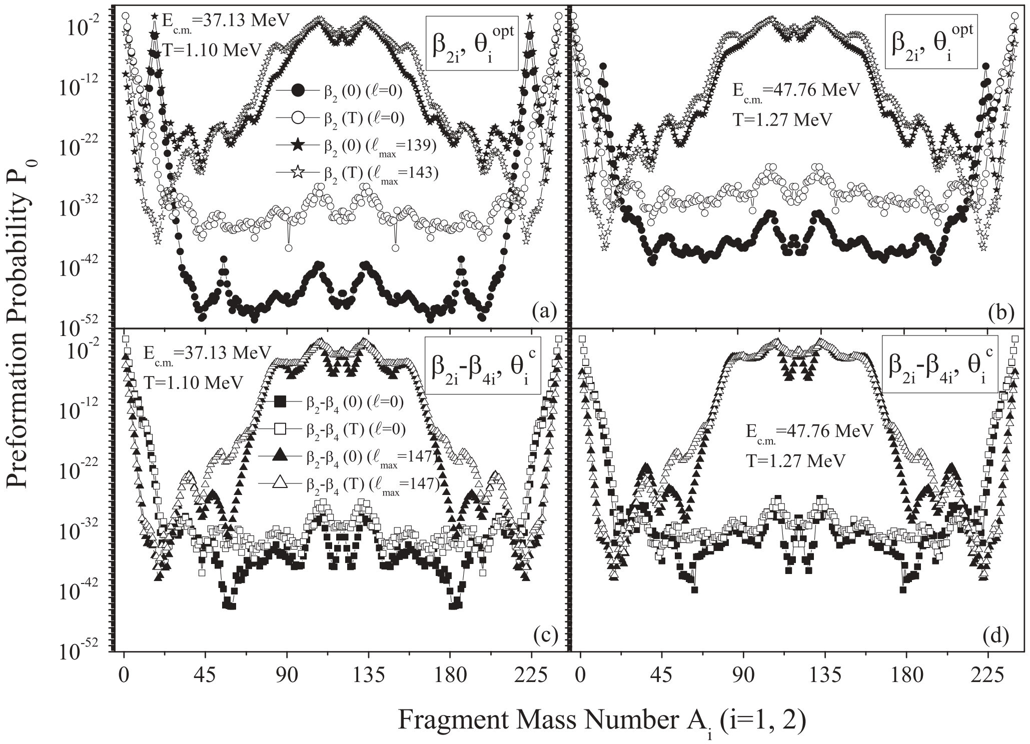

FIG. 6. Preformation probability P_0 as a function of fragment mass number A_i, $i = 1, 2$, calculated by using the fragmentation potential of Fig. 5.

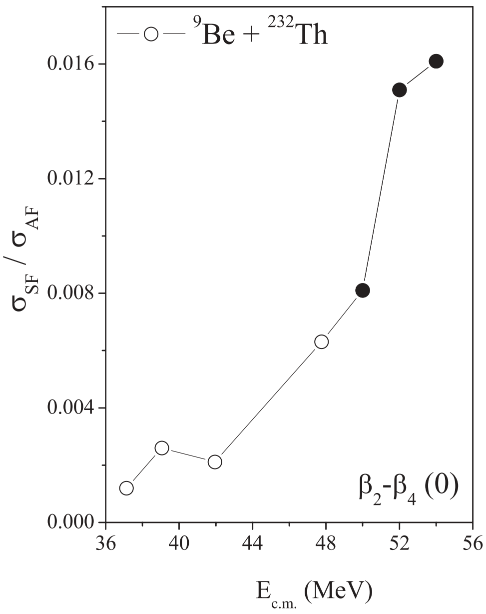

FIG. 7. The SF peak to AF peak ratio plotted as a function of the incident $E_{\mathrm{c.m.}}$ for the ^{241}Pu* compound system. The filled circles show the peak ratio at extrapolated energies.

to static or dynamical considerations in higher multipole deformations up to hexadecapole on either side of the Coulomb barrier suggest the presence of a fine structure or substructure of fission fragments. In other words, the inclusion of static and dynamical deformations in the DCM provides some new insight into the understanding of nuclear structure effects related to the decay of the ^{241}Pu* nucleus.

Figure 8 shows the ℓ-summed preformation probability P_0, penetrability P, and cross sections σ, with summation up to $\ell = \ell_{\max}$, as a function of the light-mass fragment A_2 at the highest $E_{\mathrm{c.m.}} = 47.76$ MeV ($T = 1.27$ MeV). Figure 8(a) show the results with static and dynamic deformations up to β_2 alone and Fig. 8(b) shows the same for higher multipole deformations (β_2-β_4). We note that the ℓ-summed P is almost constant and thus contributes mainly to the magnitude of the cross sections, independent of static or dynamical deformation effects for quadrupole as well as for the hexadecapole deformed fragments. Also P tends to zero for the ^{17}B fragment (and also for ^{26}Mg), which occurs as a strong minimum in the fragmentation potential of Fig. 5 or as a maximum in the preformation probability of Fig. 6. On the other hand, σ follows the behavior of P_0, which shows an interesting structure with significant preformation factors for asymmetric mass fragments. The preformation probability P_0 and penetrability P change with the inclusion of dynamical deformations, thereby affecting the compound-nucleus-decay cross sections. However, the preformation probability is more sensitive and gets strongly modified as compared to the penetrability. It may be pointed out here that the reported FF cross sections correspond to asymmetric fission ($A_{CN}/2 \pm 20$) and the fragments in the mass range $A_2 = 100$–114 seem to contribute toward fission cross sections over a wide range of incident energy; however, no individual fragments are identified in the experiment [7].

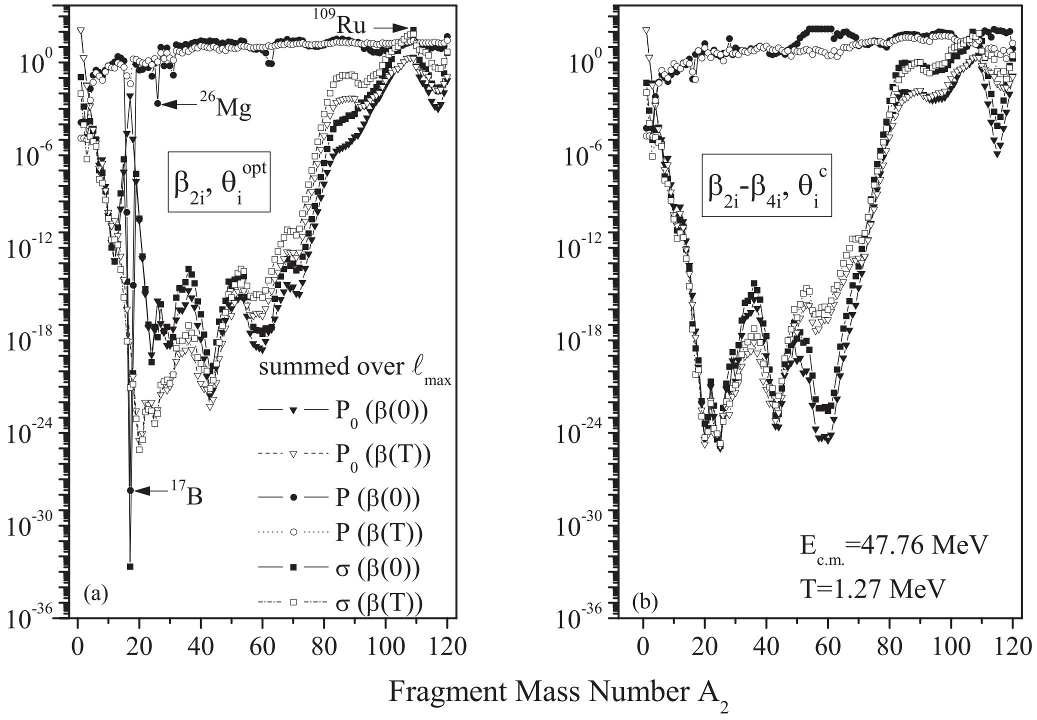

FIG. 8. The ℓ-summed preformation probability P_0, penetration probability P, and cross section σ for the decay of ^{241}Pu* as a function of fragment mass A_2 at $E_{\mathrm{c.m.}} = 47.76$ MeV for both static and dynamic choices of deformation. Part (a) shows the comparison for deformed choice of nuclei up to β_2 and part (b) shows that for deformations up to β_4.

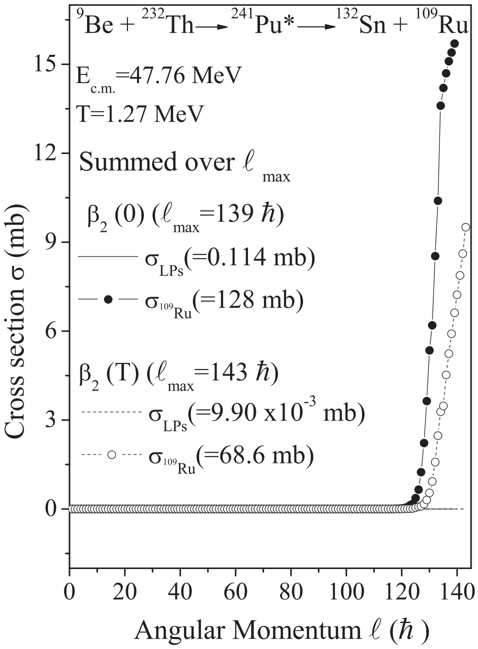

FIG. 9. Variation of cross section for an asymmetric fission fragment of mass $A_2 = 109$ ($\sigma_{A_2=109}$), and the summed cross section for LPs ($A_2 = 1$–4) (σ_{LPs}), as a function of angular momentum for the decay of ^{241}Pu*.

The above result of a favored asymmetric fragmentation in the DCM is also depicted in Fig. 9, where the DCM-calculated cross section for the LPs ($A_2 = 1$–4 summed) is compared with the most probable asymmetric fragment $A_2 = 109$ (shown in Fig. 8) alone, as a function of angular momentum, up to $\ell_{\max}$. It is clear from the figure that the contribution of the light-particle cross section σ_{LPs}, summed to $\ell_{\max}$, is almost zero compared to the cross section of the most probable asymmetric fragment for both static and dynamic deformations up to β_2 alone. Interestingly, although the $\ell_{\max}$ (=143$\hbar$) obtained for dynamical considerations up to β_2 is large, its cross section for the most probable asymmetric fragment ($A_2 = 109$) is smaller as compared to static consideration up to β_2 having a lower $\ell_{\max}$ value equal to 139$\hbar$. This occurs because the preformation probability P_0 and penetrability P for the ^{109}Ru* fragment with $\beta_2(0)$ is larger than that with $\beta_2(T)$ such that the product P_0P is larger, and hence so is the compound-nucleus-decay cross section.

Figure 10 shows the fission cross section σ_{fiss} as a function of $E_{\text{c.m.}}$ for the compound system ^{241}Pu*, calculated using the DCM and compared with the experimental data along with coupled-channel code CCFUS calculations [7]. The DCM-calculated σ_{fiss} fit the data very nicely at all energies for both static and dynamic deformations up to β_2 alone and β_2-β_4 deformed fragments. Such a nearly exact comparison between the calculations and data for both static and dynamic deformations indicate that the QF component is either small or missing. We have also calculated the σ_{LPs} contribution, which is negligibly small at all energies ($\sim 10^{-1}$ to 10^{-7} mb) and decreases with decreasing c.m. energy. This means that σ_{fiss} is the main contribution to the total decay cross section, thereby indicating the highly fissile nature of ^{241}Pu*.

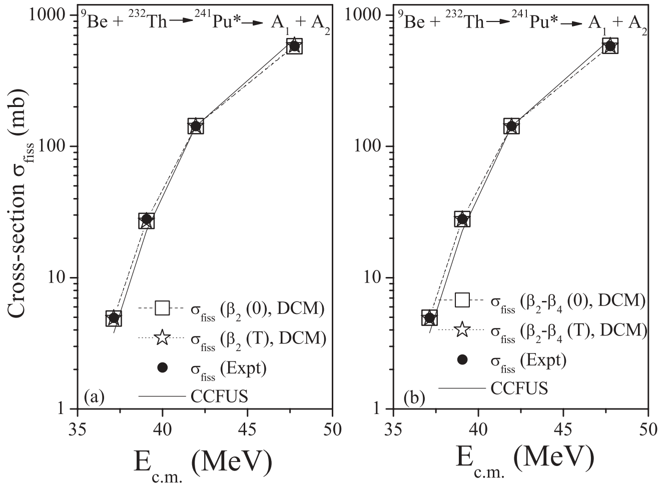

FIG. 10. The DCM-calculated σ_{fiss} for the decay of the CN ^{241}Pu* formed in the ^{9}Be + ^{232}Th reaction, compared with experimental data along with CCFUS predictions [7] for both static and dynamic choices of deformation up to (a) quadrupole (β_2) alone and (b) hexadecapole (β_2-β_4) deformed fragments.

The only parameter used to fit the data is the neck-length $\Delta R(T)[=R_a(T) - R_1(\alpha_1, T) - R_2(\alpha_1, T)]$, as shown in Fig. 11. It is to be noted that the neck-length parameter ΔR, that fixes the barrier-lowering parameter ΔV_B, for the best fit to the fission data given in Table I is found to depend strongly on the limiting $\ell_{\max}$ value, which in turn depends on whether the sticking or nonsticking limit of the moment of inertia is used for angular momentum effects in the potential. All the calculations presented above are for the sticking moment of inertia I_S, which is found to be more appropriate for fitting the fission cross sections [14]. We find that ΔR varies smoothly from above-barrier to below-barrier energies for both static and dynamic considerations. The choice of different ΔR indicates different reaction time scales for static

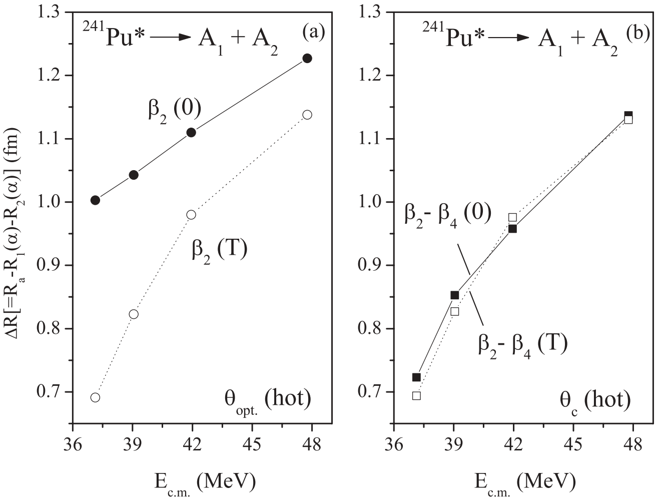

FIG. 11. The variation of fitted parameter ΔR with $E_{\text{c.m.}}$ for the fission decay of the CN ^{241}Pu* formed in the ^{9}Be + ^{232}Th reaction for both static and dynamic cases upto (a) β_2 alone and (b) β_2-β_4 deformation parameters.

TABLE I. The fission cross sections for ^{241}Pu* formed in the ^{9}Be + ^{232}Th reaction, calculated with the DCM for static and dynamic deformations up to quadrupole (β_2) alone, and up to hexadecapole (β_2-β_4), at different $E_{\text{c.m.}}$ values, compared with experimental (Expt.) data [7].

	$\beta_2(0)$ ($\ell_{\max} = 139\hbar$)		$\beta_2(T)$ ($\ell_{\max} = 143\hbar$)		β_2-$\beta_4(0)$ ($\ell_{\max} = 147\hbar$)		β_2-$\beta_4(T)$ ($\ell_{\max} = 147\hbar$)		Expt.
$E_{\text{c.m.}}$ (MeV)	ΔR (fm)	σ_{fiss} (mb)	ΔR (fm)	σ_{fiss} (mb)	ΔR (fm)	σ_{fiss} (mb)	ΔR (fm)	σ_{fiss} (mb)	σ_{fiss} (mb)
37.13	1.003	4.88	0.691	4.93	0.723	4.96	0.694	4.93	4.932
39.05	1.043	27.1	0.823	27.1	0.853	28.0	0.827	27.9	27.973
41.95	1.11	143	0.98	143	0.958	143	0.976	142	142.744
47.76	1.227	581	1.138	588	1.137	584	1.13	584	583.04

and dynamical deformations. The use of static and dynamic choices of deformation up to β_4 deformed fragments indicates almost the same value of the neck-length parameter ΔR; however, the same is not true for deformation effects up to β_2 alone, where ΔR for static deformations is much higher than that for dynamical deformations.

The barrier modification effect is also worked out as an in-built property of the fitting parameter, the neck-length parameter, shown in Fig. 12(a) as a function of $E_{\text{c.m.}}$ for the decay of ^{241}Pu* at $\ell = \ell_{\max}$ and in Fig. 12(b) as a function of ℓ at the highest c.m energy, $E_{\text{c.m.}} = 47.76$ MeV. One may observe that the barrier modification is minimum for the highest energy and becomes larger and larger as the c.m. energy decreases, with a maximum up to 10 MeV for static deformations up to hexadecapole (β_2-β_4) deformed fragments. The maximum barrier modification for dynamic deformations up to β_2 alone is ~9.5 MeV. In general, the ΔV_B value for dynamical case lies in between that for the β_2 static and the β_2-β_4 static cases. It is to be noted that the"compact" orientations change with the inclusion of temperature-dependent deformations whereas the "optimum" orientations remain intact, which means that "compact" orientations are sensitive to the magnitude of both the quadrupole and higher multipole deformations. The overall conclusion of the above calculations is that the "barrier-lowering" effect at sub-barrier energies is clearly present in the DCM irrespective of static or dynamic deformation effects.

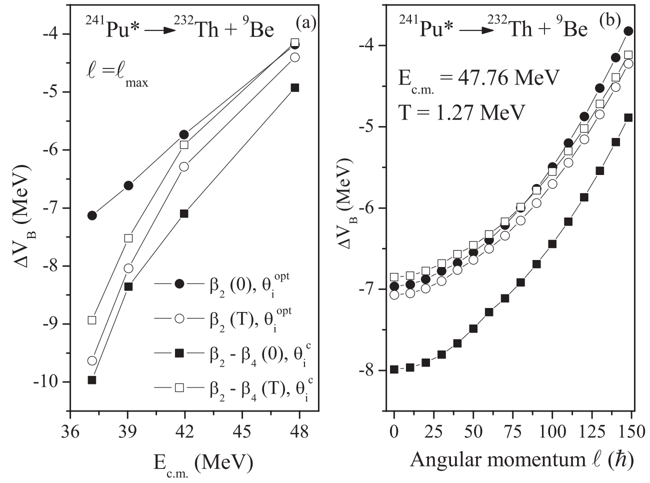

FIG. 12. (a) Barrier-lowering parameter ΔV_B as a function of $E_{\text{c.m.}}$ for the decay of ^{241}Pu* to ^{232}Th + ^{9}Be fragments, illustrated for the case of $\ell = \ell_{\max}$. (b) The same as (a) but for ΔV_B as a function of ℓ at $E_{\text{c.m.}} = 47.76$ MeV.

It is clearly evident from Fig. 12(b) that ΔV_B decreases in magnitude with the increase in angular momentum and the modification becomes small but not negligible at large values of angular momentum because with the inclusion of the ℓ-dependent potential the barrier position (R_B) starts shifting toward the left and thereby comes closer to R_a. Thus the present study clearly points out the importance of static and dynamical deformations (and orientations) in the DCM along with the explicit role played by angular momentum ℓ in the decay of the ^{241}Pu* nucleus. Since the present study is confined to a small limited energy range, the role of dynamical deformations is less pronounced here but it could be of further interest to investigate the same case over a wide range of energies spread around the Coulomb barrier, which could impart important information regarding the dynamics involved in heavy-ion reactions.

Finally, we have calculated the fission fragment anisotropies (A) using the DCM within the SSPM approach [42] [see Eq. (12)]. Note that the nonsticking moment of inertia I_{NS} corresponds to the supposition of prompt emission of fragments, used generally for the experimental determination of the ℓ value. We find that I_{NS} is more appropriate for the anisotropy calculations [14,19] whereas the sticking moment of inertia I_S is more appropriate for obtaining the fission cross sections, which has consequences for the limiting $\ell_{\max}$ value being much larger than for the nonsticking moment of inertia, i.e., I_{NS}. A comparison of $\ell_{\max}$ values from Tables I and II for the two limits of moment of inertia shows that anisotropies are fitted at a relatively much smaller $\ell_{\max}$ value, as a result of the use of the I_{NS} approach in the DCM. This is because the structure information for the fission cross section comes explicitly through the preformation probability P_0. The preformation factor being

TABLE II. The fission anisotropies calculated using the DCM for ^{241}Pu* formed in the ^{9}Be + ^{232}Th reaction, at various $E_{\text{c.m.}}$ values. Calculations here refer to the nonsticking limit of the moment of inertia.

$E_{\text{c.m.}}$ (MeV)	$\ell_{\max}$ ($\hbar$)	Anisotropy A
37.13	12	1.237
39.05	12	1.230
41.95	15	1.340
47.76	21	1.606

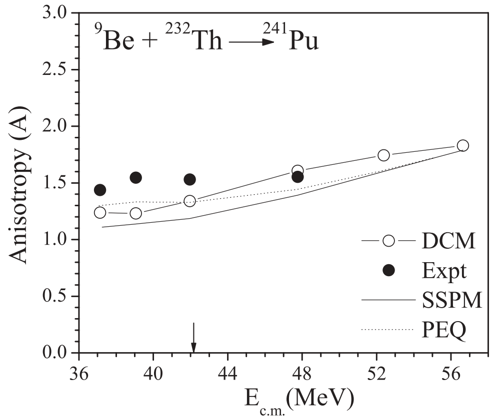

FIG. 13. The DCM-calculated fission anisotropies for the CN ^{241}Pu* formed in the ^{9}Be + ^{232}Th reaction, using the nonsticking moment of inertia I_{NS}, at various $E_{\mathrm{c.m.}}$ values compared with experimental data along with SSPM and PEQ model predictions [7]. The arrow shows the position of the Coulomb barrier.

a relative quantity in the DCM, turns out to be small or less than one for each decay product and therefore higher angular momentum values are used to address the σ_{fiss} when I_S is used.

For the calculation of anisotropy we have taken the same value of neck-length parameter ΔR as obtained for the best fit to the data on fission cross-sections with $\beta_2(0)$, where deformations are taken from the theoretical estimates of Möller *et al.* [35]. Figure 13 shows the comparison of fission anisotropies calculated using the DCM to the available experimental data along with the results of the SSPM and PEQ model predictions for the decay of the CN ^{241}Pu* at various center-of-mass energies spread across the Coulomb barrier. It may be noted here that the choice of neck-length parameter for the above-barrier predictions of SSPM anisotropy is obtained by extrapolating the values of Fig. 11 for static β_2 deformations. The behavior of the DCM-based fission-fragment anisotropies is found to be consistent with the SSPM or PEQ model (see Fig. 13). It is clear from this figure that at energies far above the barrier, the calculations are able to explain the fission anisotropy data, but they fail to reproduce the same at near- and below-barrier energies. The disagreement between the calculated and experimental anisotropies at these near- and below-barrier energies suggests a contribution from nCN fission in the reaction. The nCN fission may be attributed to QF and/or ICF processes. The excellent agreement between DCM-calculated fission cross sections and experimental data leaves very small possibility for quasifission component in the decay of ^{241}Pu*. Hence, the deviation of the theoretical estimates from the anisotropy data for ^{241}Pu* may be attributed to the possible breakup of the loosely bound projectile nucleus ^{9}Be, in agreement with Appannababu *et al.* [7].

Generally, fusion induced by a weakly bound projectile leads to two distinct processes: complete fusion, in which the entire projectile fuses with the target nucleus, and incomplete fusion, where only a part of the projectile fuses with the target nucleus. In Ref. [6] the contribution of fission cross sections comes mainly from CF since fission following ICF is expected to be negligible due to the lower angular momentum and excitation energy brought in by an ICF fragment. It would be of further interest to investigate the contribution of evaporation residues formed in the ICF process due to the breakup of the ^{9}Be nucleus into ^{8}Be + ^1n or into ^{5}He + ^{4}He in order to have a complete understanding regarding the dynamics of the fusion-fission process with stable weakly bound projectiles. It may be noted that DCM calculations are sensitive to the choice of neck-length parameter ΔR, which is taken in reference to available experimental data. In the present case the data are available only for fission cross sections and hence appropriate values of ΔR could not be estimated for ER and/or ICF paths. However, if one takes the same value of ΔR as reported in Table I for fission, then the contribution of ER or ICF remains negligibly small. In general, ΔR for ER is expected to be larger than that for fission, so the possibility of an ER and/or an ICF component in the ^{9}Be + ^{232}Th → $A_1 + A_2$ reaction is not completely ruled out. An experimental confirmation of ER and ICF data may resolve the issue.

IV. SUMMARY

The role of dynamic deformations is studied in the DCM for the ^{9}Be + ^{232}Th → ^{241}Pu* reaction at both below- and above-barrier energies. The DCM gives a good description of the fusion-fission cross sections, at various incident energies or compound nucleus excitation energies E^*, within a single parameter description ΔR for both static and dynamic choices of deformation up to quadrupole (β_2) alone and up to hexadecapole (β_2-β_4) deformations. The preformation factor P_0 is shown to get modified with the inclusion of dynamical deformations and hence the cross sections change considerably. The change in penetrability P is not as strong as that for P_0. The interesting feature of this study is that the fission mass distribution remains asymmetric, independent of static and dynamic deformation effects studied up to quadrupole β_2 or for higher order hexadecapole deformations, although a slight appearance of a symmetric peak is observed for the β_4 static case. This appearance of a symmetric peak in the fission mass distributions indicates a possible fine structure or substructure in the fusion-fission of the compound nucleus ^{241}Pu*. In order to see the possible contribution of nCN in the decay of ^{241}Pu*, calculations have also been made for the fission fragment anisotropies using the SSPM approach. The anisotropy data for the ^{9}Be + ^{232}Th reaction are underestimated by the DCM at below-barrier energies and the difference goes on decreasing with the increase in excitation energy and is consistent with the SSPM or PEQ model at above-barrier energies. The possibility of QF is ruled out and ER data are required for verification of the ICF component. The present study clearly points out the importance of static and dynamical deformations. More systematic studies regarding the dependence of deformation on temperature in different regions of fissility may be useful for an overall understanding of nuclear reaction dynamics.

ACKNOWLEDGMENTS

Financial support from the University Grants Commission (UGC) and the Department of Science and Technology (DST), New Delhi, is gratefully acknowledged.

[1] S. Kailas, Phys. Rep. **284**, 381 (1997).

[2] S. Kailas, K. Mahata, R. G. Thomas, and S. S. Kapoor, Nucl. Phys. A **787**, 259c (2007).

[3] V. S. Ramamurthy and S. S. Kapoor, Phys. Rev. Lett. **54**, 178 (1985).

[4] V. S. Ramamurthy *et al.*, Phys. Rev. Lett. **65**, 25 (1990).

[5] D. Vorkapic and B. Ivanisevic, Phys. Rev. C **52**, 1980 (1995).

[6] M. Dasgupta *et al.*, Phys. Rev. C **70**, 024606 (2004); **66**, 041602(R) (2002); Phys. Rev. Lett. **82**, 1395 (1999).

[7] S. Appannababu *et al.*, Phys. Rev. C **83**, 067601 (2011).

[8] A. Shrivastava, S. Kailas, A. Chatterjee, A. M. Samant, A. Navin, P. Singh, and B. S. Tomar, Phys. Rev. Lett. **82**, 699 (1999).

[9] B. B. Singh, M. K. Sharma, R. K. Gupta, and W. Greiner, Int. J. Mod. Phys. E **15**, 699 (2006).

[10] B. B. Singh, M. K Sharma, and R. K. Gupta, Phys. Rev. C **77**, 054613 (2008).

[11] S. Kanwar, M. K. Sharma, B. B. Singh, R. K. Gupta, and W. Greiner, Int. J. Mod. Phys. E **18**, 1453 (2009).

[12] S. K. Arun, R. Kumar, and R. K. Gupta, J. Phys. G **36**, 085105 (2009).

[13] M. K. Sharma, S. Kanwar, G. Sawhney, R. K. Gupta, and W. Greiner, J. Phys. G **38**, 055104 (2011); D. Jain, R. Kumar, M. K. Sharma, and R. K. Gupta, Phys. Rev. C **85**, 024615 (2012).

[14] M. K. Sharma, G. Sawhney, R. K. Gupta, and W. Greiner, J. Phys. G **38**, 105101 (2011); M. K. Sharma, G. Sawhney, S. Kanwar, and R. K. Gupta, Mod. Phys. Lett. A **25**, 2022 (2010).

[15] G. Sawhney and M. K. Sharma, Eur. Phys. J. A **48**, 57 (2012).

[16] M. K. Sharma, S. Kanwar, G. Sawhney, and R. K. Gupta, Phys. Rev. C **85**, 064602 (2012).

[17] M. Kaur, R. Kumar, and M. K. Sharma, Phys. Rev. C **85**, 014609 (2012).

[18] K. Sandhu, M. K. Sharma, and R. K. Gupta, Phys. Rev. C **85**, 024604 (2012).

[19] M. Kaur and M. K. Sharma, Phys. Rev. C **85**, 054605 (2012).

[20] R. K. Gupta, in *Clusters in Nuclei*, Vol. I, edited by C. Beck, Lecture Notes in Physics, Vol. 818 (Springer-Verlag, Berlin, 2010), p. 223.

[21] R. Kumar and R. K. Gupta, Phys. Rev. C **79**, 034602 (2009).

[22] R. K. Gupta, S. K. Arun, R. Kumar, and M. Bansal, Nucl. Phys. A **834**, 176c (2010).

[23] R. K. Gupta, M. Balasubramaniam, R. Kumar, N. Singh, M. Manhas, and W. Greiner, J. Phys. G **31**, 631 (2005).

[24] R. K. Gupta, M. Manhas, and W. Greiner, Phys. Rev. C **73**, 054307 (2006).

[25] M. Muenchow and W. Scheid, Phys. Lett. B **162**, 265 (1985); Nucl. Phys. A **468**, 59 (1987).

[26] M. Rashdan, A. Faessler, and W. Waida, J. Phys. G **17**, 1401 (1991).

[27] R. K. Gupta, in *Proceedings of the Fifth International Conference on Nuclear Reaction Mechanisms, Varenna*, edited by E. Gadioli (Ricerca Scientifica ed Educazione Permanente, Milano, 1988), p. 416; S. S. Malik and R. K. Gupta, Phys. Rev. C **39**, 1992 (1989).

[28] S. K. Arun, R. K. Gupta, B. B. Singh, S. Kanwar, and M. K. Sharma, Phys. Rev. C **79**, 064616 (2009); S. K. Arun, R. K. Gupta, S. Kanwar, B. B. Singh, and M. K. Sharma, *ibid.* **80**, 034317 (2009).

[29] G. Sawhney, M. K. Sharma, and R. K. Gupta, Phys. Rev. C **83**, 064610 (2011).

[30] N. J. Davidson, S. S. Hsiao, J. Markram, H. G. Miller, and Y. Tzeng, Nucl. Phys. A **570**, 61c (1994).

[31] R. K. Gupta, R. Kumar, N. K. Dhiman, M. Balasubramaniam, W. Scheid, and C. Beck, Phys. Rev. C **68**, 014610 (2003).

[32] G. Audi, A. H. Wapstra, and C. Thiboult, Nucl. Phys. A **729**, 337 (2003).

[33] W. D. Myers and W. J. Swiatecki, Nucl. Phys. **81**, 1 (1966).

[34] A. S. Jensen and J. Damgaard, Nucl. Phys. A **203**, 578 (1973).

[35] P. Möller, J. R. Nix, W. D. Myers, and W. J. Swiatecki, At. Data Nucl. Data Tables **59**, 185 (1995).

[36] H. Kröger and W. Scheid, J. Phys. G **6**, L85 (1980).

[37] R. K. Gupta, N. Singh, and M. Manhas, Phys. Rev. C **70**, 034608 (2004).

[38] G. Royer and J. Mignen, J. Phys. G **18**, 1781 (1992).

[39] T. Matsuse, C. Beck, R. Nouicer, and D. Mahboub, Phys. Rev. C **55**, 1380 (1997).

[40] S. J. Sanders, D. G. Kovar, B. B. Back, C. Beck, D. J. Henderson, R. V. F. Janssens, T. F. Wang, and B. D. Wilkins, Phys. Rev. C **40**, 2091 (1989).

[41] S. J. Sanders, Phys. Rev. C **44**, 2676 (1991).

[42] R. Vandenbosch and J. R. Huizenga, *Nuclear Fission* (Academic, New York, 1973).

[43] A. J. Sierk, Phys. Rev. C **33**, 2039 (1986).